View Article Online / Journal Homepage / Table of Contents for this issue
Dynamic Article Links

Soft Matter

Cite this: *Soft Matter*, 2011, **7**, 5799

www.rsc.org/softmatter

PAPER

Published on 16 May 2011. Downloaded by UNIVERSITA CA FOSCARI VENEZIA on 25/05/2016 13:21:06.

Two dimensional assembly of triblock Janus particles into crystal phases in the two bond per patch limit†

Flavio Romano*[a] and Francesco Sciortino*[b]

Received 15th December 2010, Accepted 22nd March 2011
DOI: 10.1039/c0sm01494j

In recent experimental work on spherical colloidal particles decorated with two hydrophobic poles separated by an electrically charged middle band (triblock Janus particles)—when particles are confined by gravity at the bottom of the sample holder—self-assembly into a Kagome two dimensional lattice has been documented [Qian Chen, Sung Chul Bae and Steve Granick, *Nature*, 2011, **469**, 381]. Here, we assess the ability of a simple two-patch effective potential to reproduce the experimental findings. The model parameters are selected to match the experimental values, with a short-range attraction mimicking hydrophobic interactions and a patch width that allows for a maximum of two contacts per patch. We show that the effective potential is able to reproduce the observed crystallisation pathway in the Kagome structure. On the basis of free energy calculations, we also show that the Kagome lattice is stable at low temperature and low pressure, but that it transforms into a hexagonal lattice with alternating attractive and repulsive bands on increasing pressure.

I. Introduction

Chemical or physical surface patterning provides an effective way of modulating the interaction between colloidal particles. The possibility of designing particles that interact *via* a non-spherical potential opens up a wealth of new possibilities, as envisioned in the anisotropy axis space by Glotzer and Solomon.[1] The challenge faced by physicists, chemical engineers and materials scientists is to organise these new geometries into structures for functional materials and devices *via* self-assembly, the spontaneous organisation of matter into desired arrangements. The aim is to achieve—*via* the rational design of elementary building blocks (*i.e.* the particles)—pre-defined specific, ordered or disordered, structures.[2] Research in this direction is very active,[3] even though most of the experimental efforts are still focused on acquiring control over the desired distribution of patch widths and numbers[4–6] more than on the collective behaviour of the particle themselves (with noteworthy exceptions[7–10]). Self-assembly of patchy particles has been the focus of a large number of theoretical and numerical investigations[1,11–18] which have revealed a wealth of novel physical phenomena, some of which have analogues in atomic or molecular systems.[19–21]

Very recent experimental work—based on spherical colloidal particles decorated with two hydrophobic poles of a tunable area separated by an electrically charged middle band (triblock Janus particles)[22]—provides an excellent example of the accurate synthesis of two-patch particles accompanied by a study of their self-assembly into an ordered structure when deposited on a flat surface. Interestingly, the electric charge of the particles allows for a controlled switch of the interaction through the addition of salt, which effectively screens the overall repulsion allowing the hydrophobic attractions between patches to gradually increase in prominence. After the addition of the salt, particles organise themselves into a Kagome lattice and their crystallisation kinetics has been followed in real space in full detail.[22] The patch width in the experimental system, of the order of 65 degrees, allows for simultaneous bonding of two particles per patch, stabilising the locally four-coordinated structure of the Kagome lattice (see Fig. 1). Experiments also show that when more than one layer of particles sediment, stacked Kagome planes form. As discussed in ref. 22, such alternating Kagome planes could have a potential application as selective filters, where selection is controlled by the two different typical sizes of the basic Kagome structure (the triangle and the hexagon) as well as by the differing chemical character of the two holes (hydrophilic and hydrophobic).

The three dimensional collective behaviour of two-patch particles, modelled by the Kern–Frenkel potential,[23] has been studied recently[24] as a function of the patch width, interpolating between the isotropic case, where each patch covers one hemisphere, and the case where each of the two opposite patches can be involved only in one bond, generating a polydisperse distribution of colloidal chains (equilibrium polymers). In the range of

[a]*Dipartimento di Fisica, Università di Roma La Sapienza, Piazzale A. Moro 5, 00185 Roma, Italy. E-mail: flavio.romano@gmail.com*
[b]*Dipartimento di Fisica and CNR–ISC, Università di Roma La Sapienza, Piazzale A. Moro 5, 00185 Roma, Italy. E-mail: francesco.sciortino@uniroma1.it*

† Electronic supplementary information (ESI) available: Supplementary information. See DOI: 10.1039/c0sm01494j

View Article Online

Published on 16 May 2011. Downloaded by UNIVERSITA CA FOSCARI VENEZIA on 25/05/2016 13:21:06.

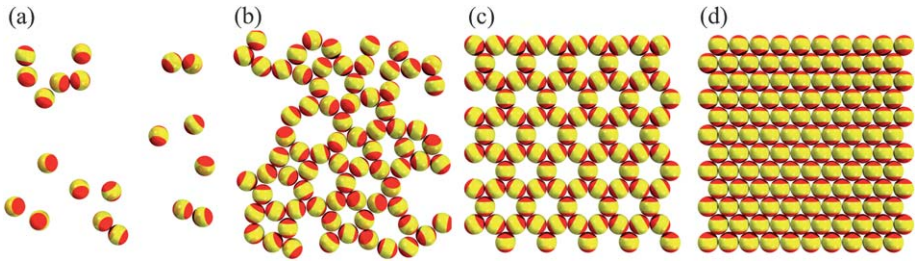

Fig. 1 From left to right: snapshot of a gas, liquid, Kagome lattice and hexagonal lattice. The Kagome and the hexagonal crystals are formed at low and high pressures, respectively. Attractive patches are coloured red; the hard-core remaining particle surface is coloured yellow. Particles are free to rotate in three dimensions, but are constrained to move on a flat surface.

patch width compatible with only two bonds per patch (analogously to the aforementioned experimental system), the spontaneous formation of an ordered phase in a fully bonded close packed hexagonal lattice with alternating attractive bands (see Fig. 1) was reported. While a close comparison between experiment and simulation in three dimensions is not currently possible, a theoretical study of the phase diagram of the same model in two dimensions—but retaining the full three dimensional orientational properties—can provide a valuable test for validating the effective potential, as well as for estimating the relative stability field of the possible crystals and of the fluid phase.

In this article, we study the phase diagram of the two-patch Kern–Frenkel model in two dimensions for two different values of the patch width, both of which are within the range of values that allows for at most two bonds per patch. In full agreement with the experiments, we observe, at comparable pressure and interaction strength, the spontaneous nucleation of a Kagome lattice. At higher pressure, spontaneous crystal formation in the dense hexagonal structure is observed. Such facile crystallisation suggests that in this system crystallisation barriers are comparable to the thermal energy at all pressures. Interestingly, we also find that for this model a (metastable) gas–liquid phase separation can be observed for large patch widths.

II. Model and simulation details

We study the Kern–Frenkel[23] two-patch model where two attractive patches are symmetrically arranged as polar caps on a hard sphere of diameter σ. Each patch can thus be visualised as the intersection of the sphere surface with a cone of aperture θ (the patch angular size being 2θ) and vertex at the centre of the sphere. In this model, a bond with interaction energy $-u_0$ is established between two particles when their centre-to-centre distance is less than $\sigma(1+\delta)$ and the line connecting their centres crosses two arbitrary patches on distinct particles.

In a formal way, the pair potential $\Phi(i,j)$ can be written as

$$\Phi(i,j) = \phi_{\mathrm{SW}}(r_{ij}) \cdot \Psi(\hat{\mathbf{n}}_i, \hat{\mathbf{n}}_j, \hat{\mathbf{r}}_{ij}), \tag{1}$$

where $\mathbf{r}_{ij}$ indicates the vector connecting the centres of particles i and j, r_{ij} its length, and $\hat{\mathbf{n}}_i$ the normalised vector that identifies the position of one patch on particle i (the other patch is thus identified by the vector $-\hat{\mathbf{n}}_i$). $\phi_{\mathrm{SW}}(r_{ij})$ is a square well potential defined as

$$\phi_{\mathrm{SW}}(r_{ij}) = \begin{cases} \infty & \text{if} \quad r_{ij} < \sigma \\ -u_0 & \text{if} \quad \sigma < r_{ij} < (1+\delta)\sigma \\ 0 & \text{if} \quad r_{ij} > (1+\delta)\sigma \end{cases} \tag{2}$$

and $\Psi(\hat{\mathbf{n}}_i, \hat{\mathbf{n}}_j, \hat{\mathbf{r}}_{ij})$ is a switch function which is equal to 1 if particles i and j have two patch favourably aligned and 0 otherwise, *i.e.*

$$\Psi(\hat{\mathbf{n}}_i, \hat{\mathbf{n}}_j, \hat{\mathbf{r}}_{ij}) = \begin{cases} 1 & \text{if} \left|\hat{\mathbf{n}}_i \cdot \hat{\mathbf{r}}_{ij}\right| \geq \cos\theta \text{ and } \left|\hat{\mathbf{n}}_j \cdot \hat{\mathbf{r}}_{ij}\right| \geq \cos\theta \\ 0 & \text{otherwise} \end{cases} \tag{3}$$

Reduced units will be used throughout this work, with $k_{\mathrm{B}} = 1$, temperature T in units of u_0/k_{B}, pressure P in units of $\sigma^{-2}u_0$ and number density ρ in units of σ^{-2}. The model has been extensively investigated in simulation and theoretical studies of patchy particles,[23–27] including integral equations[24,26] as well as perturbation theories[28] for anisotropic potentials. Here, we focus on the short–range value $\delta = 0.05$ (comparable to the experimental value) and two values of the patch width: the experimental value $\cos\theta = 0.84$ and the largest possible value consistent with the two bond per patch condition, $\cos\theta = 0.524$.

To numerically compute the free energies of the fluid and the crystals and their coexistence lines, we follow the guidelines given in a recent clear and detailed review.[29] The starting point of the procedure requires the identification of a state point in the pressure-temperature plane where two phases, I and II, share the same chemical potential, $\mu_{\mathrm{I}}(P,T) = \mu_{\mathrm{II}}(P,T)$. The chemical potential of the fluid can be computed by thermodynamic integration using the ideal gas as a reference state; this can be done by integrating the equation of state, $P(\rho)$, at fixed temperature as follows:

$$\beta f(T,\rho) = \log(\rho\sigma^2) - 1 + \int_0^{\rho} \frac{\beta P/\rho' - 1}{\rho'} \mathrm{d}\rho' \tag{4}$$

where f is the Helmholtz energy per particle; thus

$$\beta\mu(P(\rho), T) = \beta f(P(\rho), T) + \beta P(\rho)/\rho. \tag{5}$$

To compute the chemical potential of a crystal at fixed P and T, one must first compute its free energy at fixed T and ρ. Subsequent integration of the equation of state provides the chemical potential. To compute the free energy, we use the Frenkel–Ladd procedure; that is, we perform thermodynamic integration using an ideal Einstein crystal as the reference system. This procedure is described in full detail in ref. 29 and thus we do not repeat the description here. We note here that we used

 This journal is © The Royal Society of Chemistry 2011

View Article Online

Published on 16 May 2011. Downloaded by UNIVERSITA CA FOSCARI VENEZIA on 25/05/2016 13:21:06.

a standard Frenkel–Ladd[30] procedure for hard-core models with a $D_{\infty h}$-symmetric Hamiltonian in the reference Einstein crystal. We point out that in the case of the hexagonal lattice, it is particularly important to anneal all stresses in the reference configuration[31] by allowing the box side to fluctuate independently along the two directions. Coexistence lines were computed with the Gibbs–Duhem[32] integration technique using a 4th order Runge–Kutta algorithm to integrate the Clausius–Clapeyron equation starting from a coexistence point. Consistency checks based on direct coexistence[33] were performed to validate the results of free energy calculations. The gas–liquid critical point and coexistence densities were calculated using the successive umbrella sampling method.[34]

We also perform NPT and NVT Monte Carlo (MC) simulations of a system of 1000 particles for several values of P and T to gather structural information and to study spontaneous crystallisation. MC simulation runs were carried out for at least 10^6 MC cycles, a third of which were used for equilibration. The translational, rotational and volume trial displacements were calibrated during equilibration to have global acceptance ratios of 0.5, 0.5 and 0.25, respectively.

III. Results

Fig. 2 shows the phase diagram for the two investigated values of $\cos\theta$. In the range of T and P considered here, two fully bonded crystals can be predicted to form: the Kagome and the hexagonal lattices (see Fig. 1). The open Kagome structure is stable at low P and the dense hexagonal one at high P. At high T, a fluid phase is stable. We note that on increasing P beyond the range reported in Fig. 2 and outside the scope of the present article, more crystal phases appear at high T and P, including an orientationally disordered (*i.e.* not bonded) hexagonal phase and a distorted hexagonal phase with particles that are aligned to form only one bond per patch. The topology of the phase diagram is essentially identical for the two patch widths considered, with the coexistence lines shifted to higher P and higher T for the larger width as expected on the basis of the larger bonding volume (which correspondingly reflects a larger virial coefficient). In agreement with the experimental system, the Kagome structure becomes stable when the patch-patch interaction strength becomes five to ten times the thermal energy: a range of values at which bonds can still be thermally broken, providing an effective way of escaping kinetic traps and accurately sampling the phase space.

To test if the fluid phase exhibits gas–liquid phase separation at low T, we investigated the behaviour of the density fluctuations. Fig. 3 shows that the distribution of the density in the grand canonical (constant volume, temperature and chemical potential) ensemble[34] acquires the typical bimodal shape of

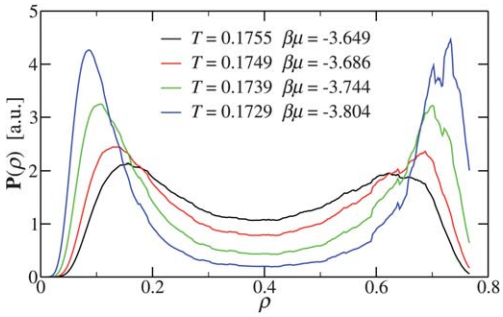

Fig. 3 Probability of the density fluctuations P(ρ) close to the metastable gas-liquid critical point for the wide-patch model ($\cos\theta = 0.524$). The formation of two different liquid-like and gas-like states in coexistence is clearly seen. Note that for $\rho > 0.8$ a third peak (not shown) corresponding to the crystal is present. For $T < 0.1729$ crystallisation is so effective that it is impossible to gather enough statistics to evaluate P(ρ).

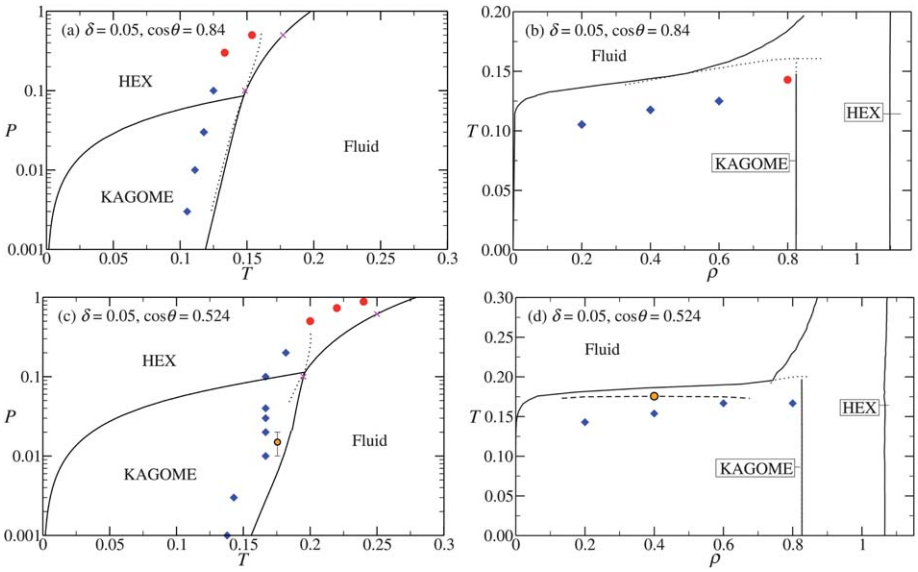

Fig. 2 Phase diagrams in the P–T plane (left column) and T–ρ plane (right column) for the narrow (top row) and wide (bottom row) patch model. Boundaries between stable phases are drawn as solid black lines and metastable phase boundaries are dotted. The orange points in panels (c) and (d) indicate the (metastable) gas–liquid critical point. The dashed line in panel (d) represents the metastable gas–liquid phase separation. Blue diamonds and red circles indicate the highest temperature at which spontaneous crystallisation into the Kagome and hexagonal lattice, respectively, was detected at the corresponding pressure or density. Crosses indicate the coexistence points checked *via* direct coexistence simulations.

View Article Online

Published on 16 May 2011. Downloaded by UNIVERSITA CA FOSCARI VENEZIA on 25/05/2016 13:21:06.

coexisting gas-like and liquid-like regions which characterize systems close to criticality. Gas configurations are characterised by small isolated clusters, while liquid-like configurations show a percolating network of bonds, with many bond loops of different sizes (see Fig. 1). The critical point, located at $T_c \approx 0.1735$ and $\rho_c \approx 0.40$, is slightly metastable (see Fig. 2). As noted in ref. 24, the progressive restriction of the bond angle plays a role analogous to the reduction of the range in spherically interacting attractive colloids.[35] Critical fluctuations can only be observed for the large angular width model. In the narrow-patch model ($\cos\theta = 0.84$) the possibility of observing the phase separation is pre-empted by crystallisation, *i.e.* crystal formation is so effective that there is no time to establish a time-independent metastable liquid state and thus to properly evaluate the density fluctuations. An appropriate choice of the patch width and interaction range in the experimental system in which particles can be optically tracked could thus provide a way of directly observing critical fluctuations in a two dimensional system in real space.

Fig. 2 also shows the points where spontaneous crystal formation in one of the two crystal forms is observed during a constant-NPT simulation. Interestingly, around $P \approx 0.1$, the Kagome crystal develops (as a metastable form) in the region of stability of the denser crystal, consistently with Ostwald's rule,[36] which states that in general it is the least stable polymorph that crystallizes first. In the present case, the difference in chemical potential between the hexagonal lattice and the Kagome lattice is only of the order of $0.03k_BT$ at $P \approx 0.1$ and $T \lesssim 0.2$ and hence can not really control the preferential crystallisation into the less stable lattice structure. We suggest that the preferential formation of the Kagome structure at $P = 0.1$ is the result of the fluid having a density closer to that of the Kagome lattice than that of the hexagonal lattice.

More relevant for colloidal applications is the phase diagram in the T-ρ plane. For the studied model, the fully bonded Kagome structure can exist only for $(\sqrt{3}/2)/(1+\delta)^2 < \rho\sigma^2 < \sqrt{3}/2$, where the upper bound is controlled by excluded volume and the lower bound by the range of the interaction potential. The Kagome structure is thus stable, strictly speaking, only in a small density window but it can nevertheless realised in a very wide density range in coexistence with an extremely diluted gas.

The crystallisation kinetics of triblock Janus particles has been investigated experimentally by optical microscopy, providing a detailed description of the formation of the Kagome lattice. To provide evidence that the Kern–Frenkel potential is able to reproduce not only the thermodynamic properties, but also the crystallisation pathway, we compare simulation and experimental data for the time evolution of the fraction of crystalline particles as well as the time dependence of the concentration of particular geometrical arrangements of the particles. Specifically, we focus (following ref. 22) on particles in chains, particles forming triangular bond loops (the unit element of the Kagome lattice), and free particles. Operationally, we identify particles that are involved in no interaction as monomers, and particles that are involved in two interactions, exactly one per patch, as chain–like. Particle i is identified as triangularly bonded if it has at least two bonded neighbours that are also bonded to each other. Fig. 4 provides a schematic example of such classification. Solid-like particles were detected by means of the two dimensional local bond order parameter ψ_6; again following ref. 22, to each particle i we assign a complex number $\psi_6(i)$, defined as

$$\psi_6(i) \equiv \frac{1}{n_i}\sum_{1}^{n_i} e^{i6\theta_{ik}} \; ; \qquad (6)$$

the index k in the sum runs over the n_i neighbours of particle i, identified as all the particles such that $r_{ik} < (1+\delta)\sigma$. i is the imaginary unit and θ_{ik} is defined as the angle between the vector $\mathbf{r}_{ik}$ and an arbitrary axis, in our case the x-axis.

The local bond order parameter ψ_6 is such that if the neighbours of particle i are placed on the vertices of an hexagon centred on particle i itself, its magnitude approaches one, while it is small if the neighbour particles are randomly placed around particle i. We identify particle i to be part of a crystalline cluster if $|\psi_6(i)| > 0.7$. The crystal is classified as Kagome if particle i has exactly four neighbours and hexagonal if i has exactly six neighbours.

Fig. 5 shows the time evolution of the number of free, chain–like and triangularly bonded particles. As time progresses, the number of free particles decreases in favour of the formation of chains of oppositely bonded particles which then restructure themselves to form the triangular elements of the ordered lattice. A movie of the crystallisation process in the numerical simulation is available in the ESI†. Comparing Fig. 5 with Fig. 2 and 3 of ref. 22, one sees that, indeed, the effective potential properly describes the kinetics of crystal formation.

Before concluding, we note that a recent study of a three dimensional tetrahedral patchy model[37] has shown that particles with narrow patches readily crystallise, while particles with wide patches never crystallise in computer simulations. Ref. 37 suggested a thermodynamic explanation based on the analysis of the

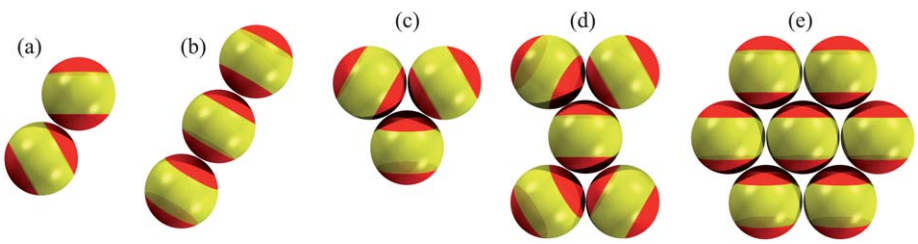

Fig. 4 Configurations identified to study the crystallisation pathway of the Kagome lattice; (a) two particles in a bonded configuration; (b) the particle in the centre is identified as chain-like since it has exactly one bond per patch; (c) all three particles are identified as triangularly bonded, since they all have two neighbours which are bonded; (d) the particle in the centre is identified as part of a Kagome lattice; (e) the particle in the centre is identified as part of a hexagonal lattice. Please note that $|\psi_6|$ is close to one in both geometries (d) and (e); classification of the crystal structure (Kagome or hexagonal) depends on the number of neighbours.

 This journal is © The Royal Society of Chemistry 2011

View Article Online

Published on 16 May 2011. Downloaded by UNIVERSITA CA FOSCARI VENEZIA on 25/05/2016 13:21:06.

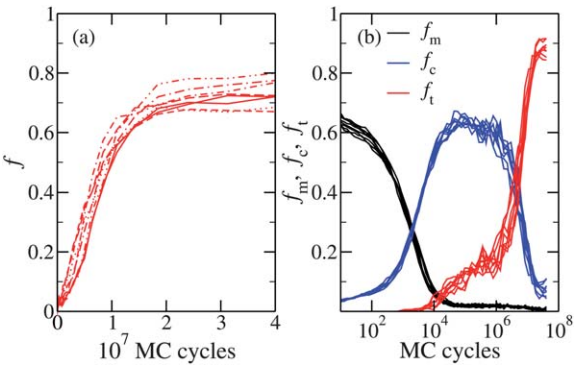

Fig. 5 Analysis of the crystallisation process of the Kagome lattice. In (a), the fraction f of solid-like particles is shown as a function of the number of MC cycles. The number of particles in a Kagome lattice exponentially approaches a plateau. In (b) the relative abundance of monomers, chain-bonded and triangularly bonded particles (f_m, f_c and f_t respectively) is shown as a function of simulation time. The crystallisation of the Kagome lattice is preceded by the formation of extensive chain-like bonding in the system. Both (a) and (b) show a striking resemblance to the experimental system. In both panels, the results of nine independent NVT runs are reported. In all the runs, $\delta = 0.05$, $\cos\theta = 0.84$, $N = 1000$, $\rho = 0.6$ and $T = 0.125$.

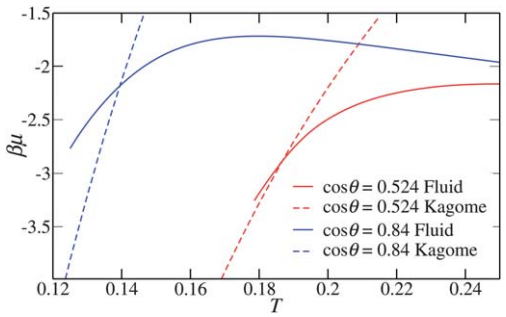

Fig. 6 Chemical potential of the fluid (solid lines) and Kagome lattice (dashed lines) for the narrow-patch ($\cos\theta = 0.84$, blue lines) and wide-patch ($\cos\theta = 0.524$, red lines) systems at $P = 0.03$. As the temperature is lowered, the difference in chemical potential between the two phases grows much more quickly in the wide–patch model.

chemical potential at constant pressure of the fluid and the crystal; in the wide-patch model, the chemical potential of the fluid and the crystal are almost parallel at coexistence and it is thus impossible to create a large enough driving force for crystallisation by undercooling the liquid. By contrast, in the narrow-patch model, the two chemical potentials have a very different slope at coexistence and thus a large driving force is created by lowering the temperature. Although in the present two dimensional model both wide-patch and narrow-patch particles crystallise, the same argument still applies. As we show in Fig. 6, the difference in $\beta\mu$ between the two phases grows much faster as the temperature is lowered below coexistence in the narrow-patch model.

IV. Conclusions and summary

To summarise, particles made by a repulsive core and attractive patches are amongst the most promising model systems for generating specific structures by rational design.[22] The versatility of the method has already been proven for one- and two-patch particles, revealing in both cases interesting assembly processes. Particles with one attractive patch aggregate in micelles or in branched linear clusters.[8,9] Interestingly, also in the one-patch case, the simple Kern–Frenkel potential has been shown to reproduce the experimentally observed structures.[38] The ability of accurately describing Janus triblock particles with the same model by only changing the patch geometry to match that of the experimental system is particularly rewarding and provides a strong support for the use of such models for predicting the self–assembly properties of this class of patchy colloids. The possibility of numerically exploring the sensitivity of the phase diagram to the parameters (patch width and interaction range) of the interaction potential provides an important instrument and a guide to the design of these new particles to obtain specific structures by self-assembly.

It is interesting to observe the analogies between the two dimensional phase diagram of these two-patch two-bonds particles with the three dimensional phase diagram of tetrahedral particles in which each patch can be engaged in only one bond.[15,16] In both cases, the phase diagram is characterised by the competition between an open (diamond in 3D, Kagome in 2D) crystal and a denser one (BCC in 3D, hexagonal in 2D). Also in both cases, narrower patches favour crystal formation, completely pre-empting the possibility of forming a metastable liquid state. Also in ref. 37, the propensity for crystallisation arises from a significant difference in the slope of $\beta\mu$ against T at the melting temperature.

In this paper, we have focused on the phase diagram of a system confined to move in two dimensions, showing that the open Kagome structure is stable at low P and T. An accurate study based on the comparison of the free energy of the different crystal forms of the corresponding three dimensional system has not yet been performed. Hence, it is not clear if the Kagome structure would still self-assemble if the system were not confined by gravity on a surface. After the validation of the model reported here, theoretical evaluation can help in answering this important question. The fact that the Kern–Frenkel model is able to provide such an accurate description of the thermodynamics and the kinetics of a fairly complex system is in our opinion due to the fact that the physics is dominated by the effects of short-range, reversible bonding. The fraction of the surface that promotes bonding is the essential parameter in describing the liquid phase,[25] while the crystal structures are dictated by the geometric arrangement of the possible crystal contacts. One clever way of tuning both these parameters is to alter the patch width, as done in ref. 22. There the choice of 65 degrees allows for no more than two contacts per particle (in two dimensions), effectively selecting the Kagome structure as the stable one at low ρ and T. A possible experimental realisation of the hexagonal lattice at higher densities, predicted by the present study, could further validate the Kern–Frenkel model as a simple and effective tool in studying the thermodynamics and the self-assembly of patchy colloids. This is particularly important in trying to exploit the potential of triblock Janus particles to self-assemble in three dimensional ordered structures, since computer simulations can greatly help in predicting the stable lattices, as well as the optimum potential parameters and ambient conditions for the self-assembly process to take place.[2]

View Article Online

Acknowledgements

We thank S. Granick for sending us ref. 22 prior to publication, C. De Michele for providing us with the program with which the graphic representations were made and A. Reinhardt for careful editing. We acknowledge support from ERC-226207-PATCHYCOLLOIDS and ITN-234810-COMPLOIDS.

References

1 S. C. Glotzer and M. J. Solomon, *Nature Mater.*, 2007, **6**, 557.
2 F. Romano and F. Sciortino, *Nature Mater.*, 2011, **10**, 171.
3 A. B. Pawar and I. Kretzschmar, *Macromol. Rapid Commun.*, 2010, **31**, 150.
4 V. N. Manoharan, M. T. Elsesser and D. J. Pine, *Science*, 2003, **301**, 483.
5 G. Zhang, D. Wang and H. Möhwald, *Angew. Chem., Int. Ed.*, 2005, **44**, 7767.
6 D. J. Kraft, J. Groenewold and W. K. Kegel, *Soft Matter*, 2009, **5**, 3823.
7 Z. Tang, Z. Zhang, Y. Wang, S. C. Glotzer and N. A. Kotov, *Science*, 2006, **314**, 274.
8 S. Jiang, Q. Chen, M. Tripathy, E. Luijten, K. S. Schweizer and S. Granick, *Adv. Mater.*, 2010, **22**, 1060.
9 L. Hong, A. Cacciuto, E. Luijten and S. Granick, *Langmuir*, 2008, **24**, 621.
10 D. Nykypanchuk, M. M. Maye, D. van der Lelie and O. Gang, *Nature*, 2008, **451**, 549.
11 E. Bianchi, J. Largo, P. Tartaglia, E. Zaccarelli and F. Sciortino, *Phys. Rev. Lett.*, 2006, **97**, 168301.
12 B. A. H. Huisman, P. G. Bolhuis and A. Fasolino, *Phys. Rev. Lett.*, 2008, **100**, 188301.
13 A. Cacciuto and E. Luijten, *Nano Lett.*, 2006, **6**, 901.
14 J. P. K. Doye, A. A. Louis, I. Lin, L. R. Allen, E. G. Noya, A. W. Wilber, H. C. Kok and R. Lyus, *Phys. Chem. Chem. Phys.*, 2007, **9**, 2197.
15 F. Romano, E. Sanz and F. Sciortino, *J. Phys. Chem. B*, 2009, **113**, 15133.
16 F. Romano, E. Sanz and F. Sciortino, *J. Chem. Phys.*, 2010, **132**, 184501.
17 A. W. Wilber, J. P. K. Doye and A. A. Louis, *J. Chem. Phys.*, 2009, **131**, 175101.
18 A. W. Wilber, J. P. K. Doye, A. A. Louis and A. C. F. Lewis, *J. Chem. Phys.*, 2009, **131**, 175102.
19 F. Sciortino, *Eur. Phys. J. B*, 2008, **64**, 505.
20 J. Russo and F. Sciortino, *Phys. Rev. Lett.*, 2010, **104**, 195701.
21 J. Russo, J. M. Tavares, P. I. C. Teixeira, M. M. Telo da Gama and F. Sciortino, *Phys. Rev. Lett.*, 2011, **106**, 085703.
22 Q. Chen, S. C. Bae and S. Granick, *Nature*, 2011, **469**, 381.
23 N. Kern and D. Frenkel, *J. Chem. Phys.*, 2003, **118**, 9882.
24 A. Giacometti, F. Lado, J. Largo, G. Pastore and F. Sciortino, *J. Chem. Phys.*, 2010, **132**, 174110.
25 G. Foffi and F. Sciortino, *J. Phys. Chem. B*, 2007, **33**, 9702.
26 A. Giacometti, F. Lado, J. Largo, G. Pastore and F. Sciortino, *J. Chem. Phys.*, 2009, **131**, 174114.
27 H. Liu, S. K. Kumar and F. Sciortino, *J. Chem. Phys.*, 2007, **127**, 084902.
28 C. Gogelein, G. Nagele, R. Tuinier, T. Gibaud, A. Stradner and P. Schurtenberger, *J. Chem. Phys.*, 2008, **129**, 085102.
29 C. Vega, E. Sanz, J. L. F. Abascal and E. G. Noya, *J. Phys.: Condens. Matter*, 2008, **20**, 153101.
30 D. Frenkel and A. J. C. Ladd, *J. Chem. Phys.*, 1984, **81**, 3188.
31 E. G. Noya, M. M. Conde and C. Vega, *J. Chem. Phys.*, 2008, **129**, 104704.
32 D. A. Kofke, *Mol. Phys.*, 1993, **78**, 1331.
33 A. J. C. Ladd and L. Woodcock, *Chem. Phys. Lett.*, 1977, **51**, 155.
34 P. Virnau and M. Müller, *J. Chem. Phys.*, 2004, **120**, 10925.
35 G. A. Vliegenthart and H. N. W. Lekkerkerker, *J. Chem. Phys.*, 2000, **112**, 5364.
36 W. Ostwald, *Z. Phys. Chem.*, 1897, **22**, 289330.
37 F. Romano, E. Sanz and F. Sciortino, *J. Chem. Phys.*, 2011, **134**, 174502.
38 F. Sciortino, A. Giacometti and G. Pastore, *Phys. Rev. Lett.*, 2009, **103**, 237801.

Published on 16 May 2011. Downloaded by UNIVERSITA CA FOSCARI VENEZIA on 25/05/2016 13:21:06.

 This journal is © The Royal Society of Chemistry 2011